Journal of Quantitative Spectroscopy & Radiative Transfer 265 (2021) 107544

Contents lists available at ScienceDirect

Journal of Quantitative Spectroscopy & Radiative Transfer

journal homepage: www.elsevier.com/locate/jqsrt

Accurate determination of the onset wavelength (λ_{onset}) in optical spectroscopy

Austin M. Wallace, Christine Curiac[1], Jared H. Delcamp, Ryan C. Fortenberry*

Department of Chemistry & Biochemistry, University of Mississippi, University, MS 38677-1848, United States

ARTICLE INFO

Article history:
Received 16 November 2020
Revised 25 January 2021
Accepted 27 January 2021
Available online 1 February 2021

Keywords:
Spectral lineshapes
Computational algorithms
Electronic spectroscopy
Data processing

ABSTRACT

Human attribution of absorption onset wavelength (λ_{onset}) most often produces small, but non-negligible errors in the attribution of this value tied to the optical energy gap. The present work utilizes a free and freely available computer program ("0nset") developed herein to determine the inflection point and subsequent x-intercept defining λ_{onset}. The manually attributed absorption curve λ_{onset} wavelengths are typically in error to the red (in 27 out of 38 attributions) for the dataset utilized in the present work when a rigorous manual analysis was performed implying a systematic human error. The raw (−2 nm) and absolute (3 nm) errors are relatively small, but there are exceptions when the errors are even larger than 20 nm. The numerically computed results from 0nset are independent of application bias and will reduce errors moving forward by consistently generating λ_{onset} values from the same algorithm. Additionally, it will reduce errors in circumstances where the inflection points are difficult to isolate or in regions like the UV where ~5–10 nm errors are more significant energetically. Finally, 0nset only requires .csv inputs and is built for both Windows and Unix-based operating systems making uptake and usage straightforward for experimental groups.

1. Introduction

The onset wavelength (λ_{onset}) is a convenient heuristic for determining underlying physical properties of a compound based solely on optical spectral data [1]. The value of λ_{onset} is often defined as the x-intercept of a tangent line (or line of best fit) on the inflection point for the lowest energy absorption transition of a compound regardless of whether the lowest energy transition is the highest intensity peak in the spectrum or not [2]. The onset wavelength is meant to be an approximation of the $E_{(0-0)}$ optical energy gap interpreted as the intersection of the absorption and emission curves for singlet state emitting materials [3]. Non-emissive (case 1) and low energy absorbing materials that weakly emit beyond Si-detector or photomultiplier tube limits (case 2) often inherently require estimation of the optical energy gap as shown in Fig. 1. Similarly, triplet emitters with facile intersystem crossing require the use of a tangent line fit on the high energy side of the emission curve to approximate excited state energy levels since singlet state absorption-triplet state emission curve crossing is non-informative, case 3 from Fig. 1.

Beyond absorption and emission spectroscopy, several additional types of data require the use of onset value determination via lines of best fit typically manually drawn onto the data samples. Examples with this analysis published in the literature include articles on thermalgravimetric analysis (TGA), [4] differential scanning calorimetry (DSC), [5] Tauc plot analysis, [6,7] X-ray/ultraviolet photoemission spectroscopy (XPS/UPS), [8–12] and inverse photoemission spectroscopy (IPES) [11–13].

Moreover, the onset wavelength is used to quantitatively predict an approximate optical gap of the compound [14] by utilizing the equation:

$$E_g^{opt} = \frac{hc}{\lambda_{onset}} \quad (1)$$

The product of h and c, Planck's constant and the speed of light, respectively, is typically approximated to 1240 nm. As a result, λ_{onset} is a straightforward value determined from observed properties that do not require more detailed analysis beyond an optical absorption characterization [15]. Materials applications for such a property range from solar energy production to light emitting diodes to photocatalysis among many other uses for materials utilizing the emission or absorption of photons.

* Corresponding author.
E-mail address: r410@olemiss.edu (R.C. Fortenberry).
[1] Co-First Author.

https://doi.org/10.1016/j.jqsrt.2021.107544
0022-4073/

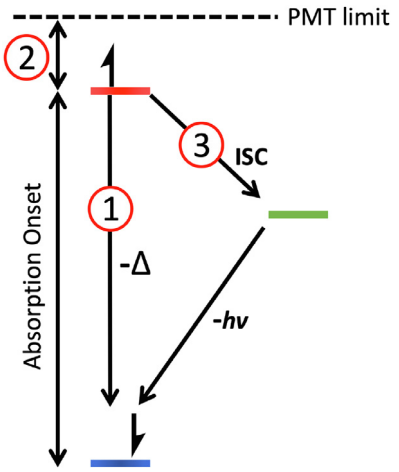

Fig. 1. Three examples where absorption and emission intercepts ($E_{(0-0)}$) are non-obtainable. Case 1: The material is non-emissive. Case 2: The emission is beyond detector or photomultiplier tube limits for the instrument available. Case 3: Inter-system crossing (ISC) occurs resulting in the excited state energy lowering and being non-informative relative to the absorption energy.

As applicable as utilizing λ_{onset} to determine E_g^{opt} is, a generally accepted, rigorous means of determining this value has not been determined. Again, λ_{onset} is most often determined manually. In some cases, the spectrum is projected onto a screen, and a meterstick is stretched from the perceived inflection point to the x-axis in order to determine this intercept. Even when straight lines are applied to an absorption or emission curve visually on a computer screen, proper selection of the inflection point or creation of an approximate tangent line is only accurate within a certain window. Additionally, λ_{onset} is often determined by simply observing where the curve nears zero on the x-axis. Likely the largest error introduction is with this approach. As a result, the determination of λ_{onset} is fraught with human errors and is reminiscient of cutting out paper readouts of NMR spectra and weighing the actual paper to get relative areas for comparison [16]. While such practices were state-of-the-art in the middle of the last century, computer analysis of standard spectral output has revolutionized NMR spectroscopy through numerical integration of the peak areas [16,17]. Similarly, computationally determining an optical spectrum inflection point and tangent line is straightforward with modern tools (even though it is currently not standard practice) and should make finding λ_{onset} not only more accurate but also more convenient and consistently approximated within the research fields that utilize this metric.

Additionally, λ_{onset} and its closely-related optical energy gap are challenging to obtain in some instances, especially when working with weakly emissive compounds. This could be due to the intrinsic optical properties for the compound of interest or even due to the spectral region where the lowest energy transition occurs. Projector and meterstick (or digital line and computer screen) analysis breaks down quickly when the peaks are short and wide making the inflection point difficult to isolate [2]. Furthermore, "eyeballing" λ_{onset} is easily skewed when moving into the UV region where the difference of a few nm could be on-the-order of 0.5 eV or more [18]. Numerical analysis can find the proper inflection point and corresponding x-intercept regardless of the peak height, width, or region of the spectrum.

Consequently, a more robust method is needed in optical materials research fields. The tool utilized must interface easily with existing experimental data outputs, work on the sub-second time scale, and be user-friendly enough so that it can have ready uptake by practioners in the field who are already inundated with dozens of tools. Hence, this paper will present such a program (called "0nset") and comment on the attribution of recently reported λ_{onset} values from the literature compared with results computed by 0nset. This program should reduce the errors (or at least systematize results) for λ_{onset} attribution by introducing a new, user-friendly computational paradigm for analysis.

2. The "0nset" program

The "0nset" program operates on a local host and runs a Python-Flask application through an executable file. The program takes a zeroed baseline dataset in the form of a .csv file and calculates the λ_{onset} after the longest wavelength/lowest energy peak or shoulder in the data. Manual input ranges enable users to choose different ranges from the dataset, and the x-direction feature permits the selection of either side of the local maximum for finding a λ_{onset} line. After selecting the units, clicking the "upload file" button will display a graph with the data and the functional form of the line used to calculate the λ_{onset}. Additionally, this page displays the polynomial fit used for calculating the derivatives and allows users to save a figure with user-specified modifications to the axis, ranges, λ_{onset} line existence, filename, and title.

The program extracts the rows and columns of the data from the file and finds the maximum within the given range. In order to ensure that the plotted lines match the data in a future step, the y-values are all divided by the maximum y-value normalizing the functional ordinate. The program then runs the algorithm several times in the background shifting the input range up to form several λ_{onset} lines from different polynomial fittings. The fourth degree polynomial fitting slightly changes the onset value; therefore, several shifted ranges are used to form a more accurate and reproducible output. The onset lines are determined through calculating the numerical first and second derivatives over the shifted input ranges to find the inflection point.

After the algorithm plots several lines (which are not presented to the user), the lines are evaluated based on their slope's steepness and how well the line fits the original dataset within 15 data points from the inflection point. The matching is determined through a list of booleans produced by *numpy.isclose*(), which uses the evaluation $absolute(a - b) \leq (atol + rtol * absolute(b))$ where $rtol$=*1e-06* and $atol$=*1e-02*. The total number of Trues are summed to be the matches. The line with the highest value from the equation $value = (matches) - 1500 * (slope)$ is used as the final λ_{onset} line. Due to normalizing the maximum absorption data point to 1.0, the evaluation will work regardless of units provided in the input dataset. If the original units are desired for display, then the option can be selected under the "Y Values" dropbox in the input page.

The equation of the line is acquired through plotting a line that passes through the inflection point with the slope determined by the first derivative at that point and the y-intercept coming from the original function at that point. Then, the line is translated to pass through the inflection point, and where the onset value is reported as the x-intercept of the final line generated.

Although the program can find an onset after the longest wavelength peak without manual input ranges, the program should be run again with manual input ranges to ensure that the desired peak is selected and that the polynomial fitting finds the appropriate inflection point. For example, Fig. 2 displays the the output graph for the molecule C5 with a phosphorus hexafluoride counterion in the solid state [15]. When the program is run with no manual ranges - the "Minimum X Value" and "Maximum X Value" both are "0.0" - it finds the maximum in the dataset and the next inflection point. In this example, the initial estimate over the entire range of the data places the λ_{onset} at 851 nm. However, a more sensible, yet still large, range (800 nm to 900 nm) encom-

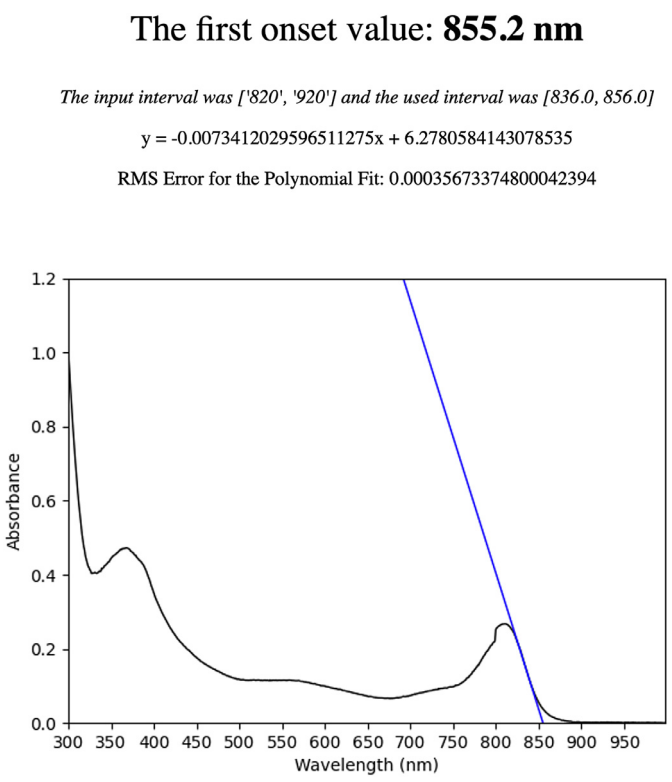

Fig. 2. 0nset determination of λ_{onset} for a thin film of C5 with a wide input range.

passes the entire low-energy side of the curve produces a minimally shifted λ_{onset} of 855 nm as shown in Fig. 2. Further refinements to a smaller range do not change this onset wavelength. The units are also variable; nm, cm^{-1}, and eV are currently available.

Consequently, after a first attempt, the user should define a manual input range that starts before the local maximum of the desired peak without including a higher maximum before the peak so as to isolate the actual curve feature of interest. Next, the minimum should be a point after the local minimum. This provides a large enough range for the program to make several polynomial fits in order to ensure the best λ_{onset} line is selected and that it contains the true inflection point in the data. Using AP14 as an example in Fig. 3, the initial guess without a data range does not produce the proper inflection point and the corresponding λ_{onset} value is not near a sensible range. However, it permits the user to see the graph and what interval the program selected for the input range. The input page in the top of Fig. 4 shows the selected input range for this dataset and the output shows the correct λ_{onset} line through the appropriate inflection point. Therefore, the process should be to first run the program without an input range and then run it again with a more defined range for a particular peak.

3. Analysis approach

In order to assess the proficiency for the "0nset" program, 38 previously attributed λ_{onset} values and their associated spectra have been taken from the literature and from our group. The "0nset" computed λ_{onset} values are determined by utilizing the above approach where an initial run produces an estimated x-intercept for consideration before the range containing the inflection point is limited by the user. This results in much better behaved tangent lines as the example of AP14 has highlighted in Figs. 3 and 4.

The differences in the previously attributed and the presently computed λ_{onset} values are reported in this work. The raw differences are averaged as well as the absolute values of the differences where the latter gives the mean absolute error or MAE. Percent differences are also computed as the difference in the numerator and the previously attributed λ_{onset} as the denominator. This is interpreted to show how much error in the manual attributions may result.

4. Results and discussion

Table 1 reports a list of 38 different λ_{onset} values taken from the recent literature as produced in the Delcamp group and the corresponding 0nset-computed values from this present work. The entries selected include organic dyes with high energy charge transfer bands ($\lambda_{onset} \leq 500$ nm), organic dyes with low energy charge transfer bands ($\lambda_{onset} \geq 600$ nm), organic cyanine-type absorption spectra (750 nm $\leq \lambda_{onset} \leq$ 1020 nm), and metal-to-ligand charge transfer transition metal complexes. A variety of spectral shapes are represented here with some broad charge transfer transitions and sharp cyanine type transitions. Spectra with and without shoulders as the low energy transition are purposefully selected to probe the capabilities of the 0nset program. The MAE for the difference is 3 nm. The raw average is −2 nm. The percent errors, which are agnostic to the region of the spectrum involved, have averages of 0.55% and −0.24%, respective of absolute and raw datasets. The previously manually-attributed λ_{onset} values are typically reported in 5 nm increments, and the errors, regardless of raw or absolute, are on the order of such an increment. While the overall averages do not produce a large error on average, the range of error deviates from the average to 11 nm in $Mn(bpy)_2Br_2$ to −29 nm in $Ir(ppy)_3$, or 2.29% to −5.92%, respectively, in our set.

Some λ_{onset} attributions appear to be more straight-forward than others. For instance, C5 with PF_6 [15] is identical between the attributed experimental and the computer-analyzed λ_{onset} results. However, the raw average of the difference between the previously attributed and the 0nset λ_{onset} is negative, with 27 of the 38 differences in Table 1 resulting in negative values. This indicates that the observer is most often subconsciously inclined to artificially red-shift the attributed λ_{onset} consequently producing a smaller E_g^{opt} and underestimating the optical energy gap. Such a difference could lead to difficult and time-consuming synthesis of boundary pushing materials that may not have the needed properties for the desired application. This would result, then, in a significant inaccuracy for many optoelectronics applications.

Whether the human determination of the inflection point itself or "eyeballing" of the slope of the tangent line (or a combination of the factors) is the cause for this common error is unclear. The 38 entries in our dataset have, in large part, been synthesized with aims of creating longer wavelength absorption/emission properties. This objective could also be shifting the results by a subconscious desire from the observer to create materials with λ_{onset} values more toward the red. In any case, the remedy for this seemingly systematic error is to utilize a non-biased computational analysis to determine the λ_{onset} value in the future.

$E_{(0-0)}$ is generally the preferred method of determining optical energy gap values when measurable. However, when these values can not be obtained, alternative optical energy gap estimations are used with line of best fit and 10% absorbance peak height measurements being the most commonly employed (Fig. 5). Many researchers prefer the 10% peak height method due to the lack of ambiguity or human error in obtaining the value. However, with computerized approaches, this ambiguity can be eliminated. We are unaware of a systematic study comparing the two methods without potential human bias. For all of the cases with experimental $E_{(0-0)}$ data available (31 dyes), the average 0nset and

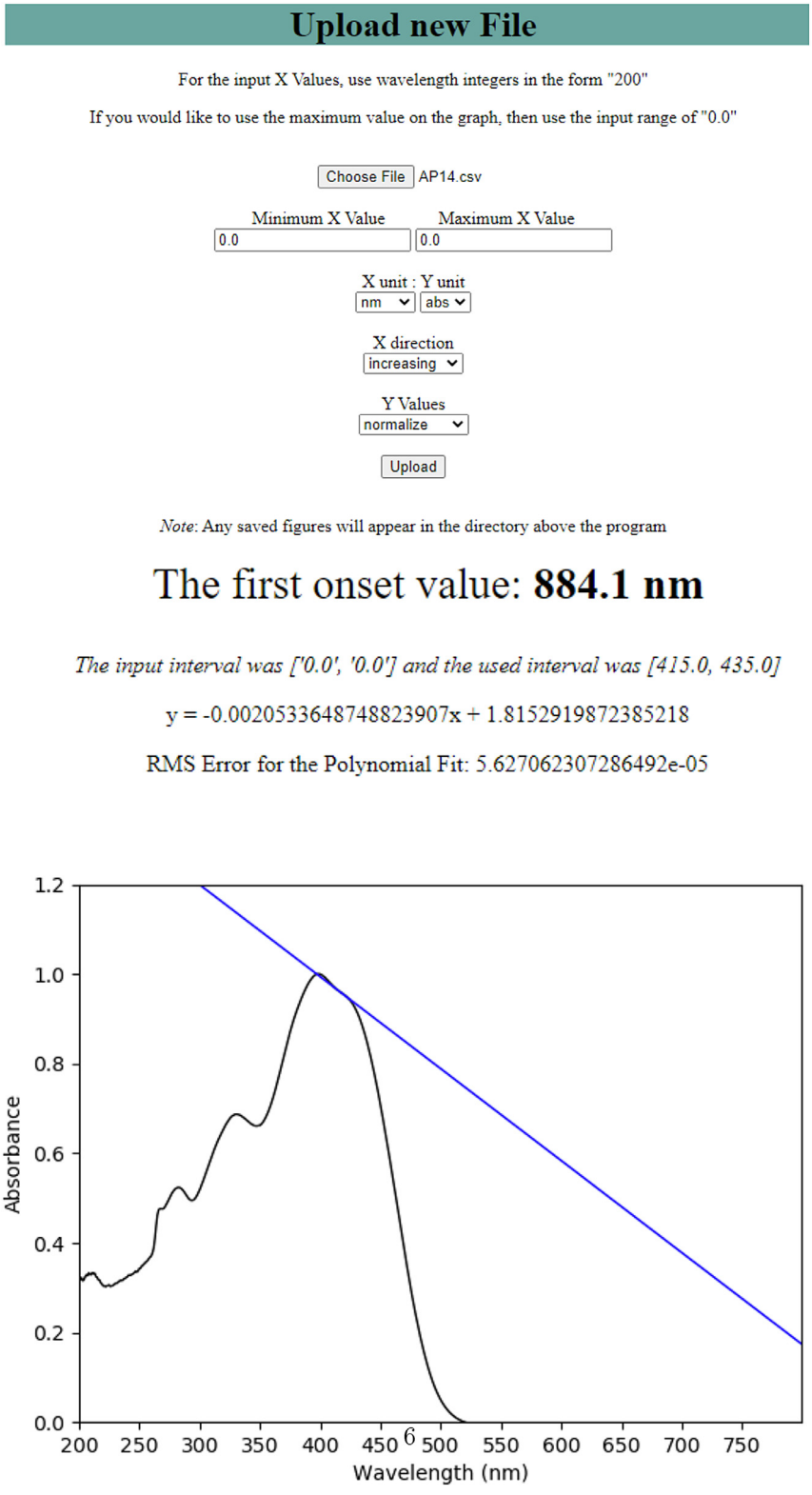

Fig. 3. The starting input screen on the top and the output graph on the bottom.

10% height values are compared. On average, the 0nset values are within 19 nm (0.05 eV) of the $E_{(0-0)}$ values. In all cases except one, the 0nset values are red-shifted relative to the $E_{(0-0)}$ values. Comparatively, the use of 10% half height values results in a less correlated value to $E_{(0-0)}$ than 0nset with red-shifts on average of 31 nm (0.07 eV). Notably, the 10% height analysis and the human estimated line of best fit method give substantially different values (40 nm or a 0.18 eV difference) when comparing values on curves with overlapping features such as in the case of W(pyNHC)$(CO)_4$ (Fig. S34).

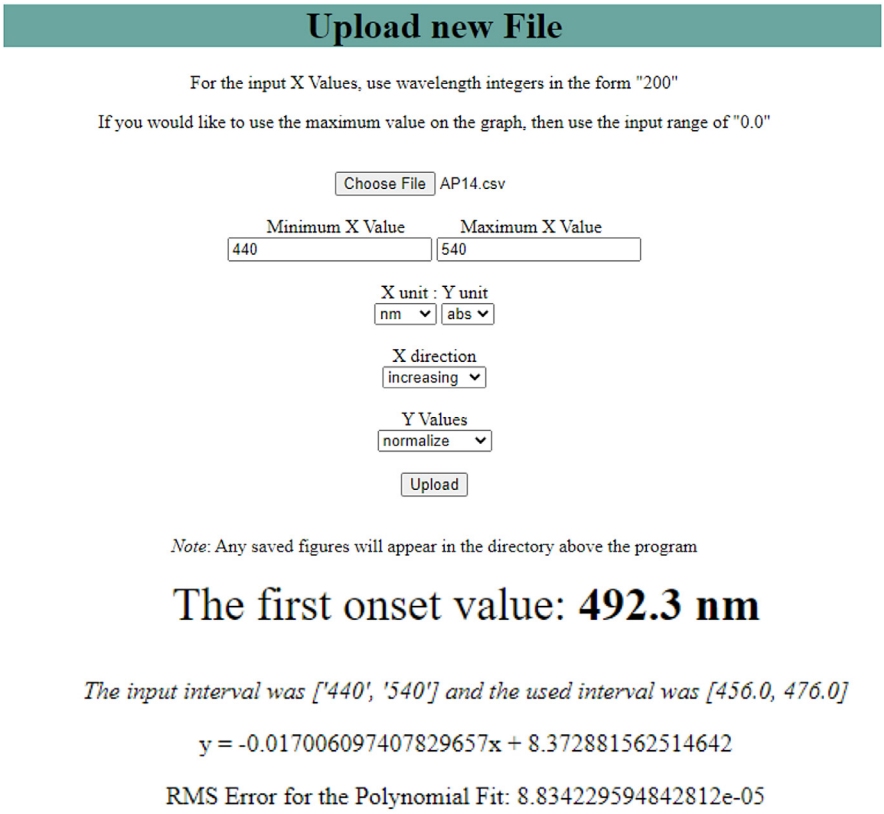

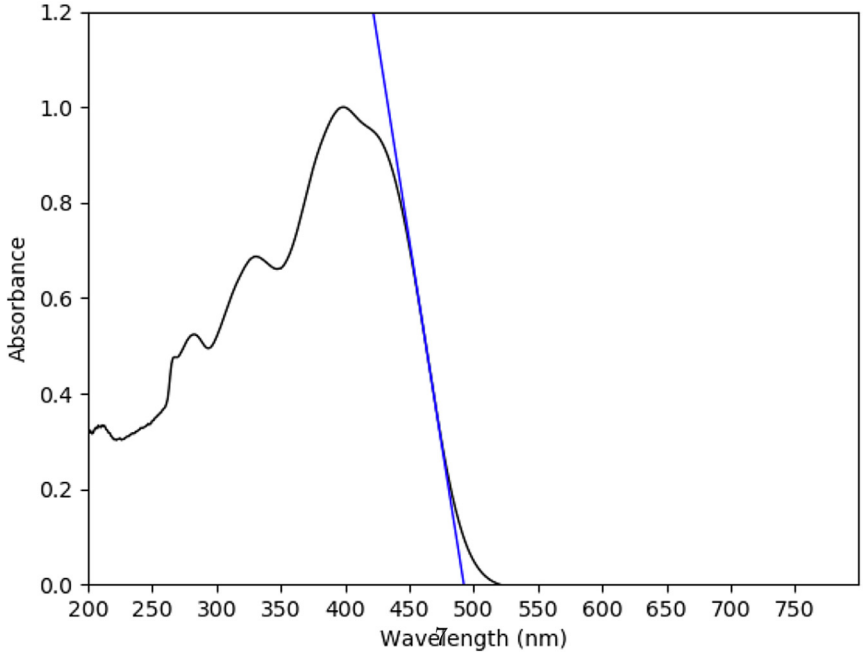

Fig. 4. The modified input screen on the top and the output graph on the bottom.

Finally, the applicability of the 0nset program toward emission curve λ_{onset} estimations on the high energy side of the curve are shown in Fig. 6. This analysis is important since non-singlet state emitters often have the first triplet excited state energy level (T_1) values estimated from the emission curve rather than the absorption curve as was used in all of the prior examples. The λ_{onset} of the emission curve is an applicable method of estimating the energetic distance from the T_1 to the ground state energy level (S_0) for compounds exhibiting intersystem crossings (Fig. 1, case 3). $Ir(ppy)_3$ provides a key example of the utility of the 0nset program.

Table 1
Comparing the Previously Attributed and Computed λ_{onset} Values (in nm). See Fig. S43 for dye structures.

Dye	Reported	0nset Value	10% Height	$E_{(0-0)}$	Diff.[a]	Percent Diff. (%)	Reference
C5 w/ TFSI in DCM	875	872	876	850	−3	−0.34%	[15]
C5 w/ BARF in DCM	875	871	876	847	−4	−0.46%	[15]
C5 w/ Cl in DCM	870	869	875	840	−1	−0.11%	[15]
C5 w/ NO_3 in DCM	870	871	878	846	1	0.11%	[15]
C5 w/ PF_6 in DCM	870	870	876	848	0	0.00%	[15]
C5 w/ TPB in DCM	875	870	876	851	−5	−0.57%	[15]
PhIndzC1 in 1:1 MeCN/H_2O	695	699	702	669	4	0.58%	[19]
PhIndzC3 in DMSO	740	739	744	720	−1	−0.14%	[19]
PhIndzC5 in MeCN	855	854	859	786	−1	−0.12%	[19]
IndzOMe-C5 in DMSO	885	880	884	853	−5	−0.56%	[19]
PhCN-C5 in DCM	880	879	883	848	−1	−0.11%	[19]
PhOMe-C5 in DMSO	870	867	872	830	−3	−0.34%	[19]
PB1 in DCM	650	648	656	585	−2	−0.31%	[20]
AP11 in DCM	470	470	464	476	0	0.00%	[21]
AP14 in DCM	495	496	493	493	1	0.20%	[21]
AP16 in DCM	475	477	473	446	2	0.42%	[21]
AP17 in DCM	455	453	452	441	−2	−0.44%	[21]
bisCF_3PhIndzSQ in toluene	745	744	751	735	−1	−0.13%	[22]
*bis*tBuOH PhIndzSQ in toluene	740	736	744	726	−4	−0.54%	[22]
CF_3PhIndzSQ in toluene	750	749	762	738	−1	−0.13%	[22]
CNPhIndzSQ in toluene	755	752	764	734	−3	−0.40%	[22]
MesPhIndzSQ in toluene	745	743	754	725	−2	−0.27%	[22]
NaphIndzSQ in toluene	755	753	767	740	−2	−0.26%	[22]
OH PhIndzSQ in DMSO	755	752	770	726	−3	−0.40%	[22]
OMe PhIndzSQ in toluene	750	748	768	731	−2	−0.27%	[22]
PhIndzSQ in toluene	750	748	764	731	−2	−0.27%	[22]
PyrIndzSQ in toluene	750	750	761	736	0	0.00%	[22]
RhIndz in DCM	1040	1033	1044	1004	−7	−0.67%	[23]
$Mn(bpy)(CO)_3Br$ in MeCN	480	491	482	non-emissive	11	2.29%	[24]
$Mn(bpy)_2Br_2$ in MeCN	455	451	465	non-emissive	−4	−0.80%	[24]
ICG in MeOH	830	829	835	804	−1	−0.12%	[25]
SO3C5 in MeOH	850	848	858	805	−2	0.24%	[25]
SO3SQ in MeOH	735	731	744	710	−4	−0.54%	[25]
$W(pyNHC)(CO)_4$ in MeCN	450	446	540	non-emissive	−4	0.89%	[26]
AP25 in DCM	765	761	770	N/A[b]	−4	−0.52%	[27]
$Ru(bpy)_3Cl_2$ in MeCN[c]	550	551	549	triplet emitter	1	0.18%	[28]
$Ir(ppy)_3$ in MeCN (410 nm)[c,d]	480	480	477	triplet emitter	0	0.00%	[28]
$Ir(ppy)_3$ in MeCN (490 nm)[c,d]	490[e]	461	N/A[f]	triplet emitter	−29	−5.92%	[28]
Raw Average					−2	−0.24	
Absolute Average					3	0.55	

[a] Difference taken between the 0nset value and the reported value.
[b] Beyond photomultiplier tube ~850 nm detection limit.
[c] Data is reported from the emission curve on the high energy side.
[d] The emission maxima and low energy onset shifts with a change in excitation energy.
[e] Rough estimation due to minimal curve shape observed on the high energy side of the emission due to overlap with the excitation signal.
[f] Not observable due to overlap with the excitation signal.

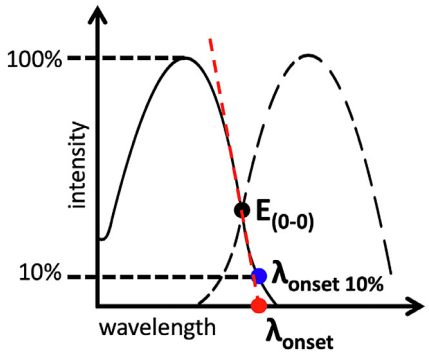

Fig. 5. An illustration of the two methods, 10% absorption peak height ($\lambda_{onset\ 10\%}$) and line of best fit (λ_{onset}), commonly used in the literature to approximate $E_{(0-0)}$ values when $E_{(0-0)}$ values cannot be obtained.

$Ir(ppy)_3$, when excited at 490 nm, results in an emission λ_{onset} estimate at 461 nm via the 0nset program. The higher energy emission than excitation observed by the compound is due to the photoexcitation of an electron in a higher S_0 vibrational energy level followed by an emission to a lower S_0 vibrational energy level. As with any compound that participates in intersystem crossing, the absorption and emission transitions are from different spin states which does not allow for the use of $E_{(0-0)}$ values if the curves cross. Thus, the use of the 0nset program is attractive for estimating the T_1 energy level. When finding the emission curve λ_{onset}, the high energy side is used which 0nset is amenable to with a simple selection click for x-axis direction shift set to "decreasing." Fig. 6 shows the emission curve obtained with $Ru(bpy)_3Cl_2$ with a human estimated onset value of 550 nm. The 0nset estimation is in close agreement with this value at 551 nm.

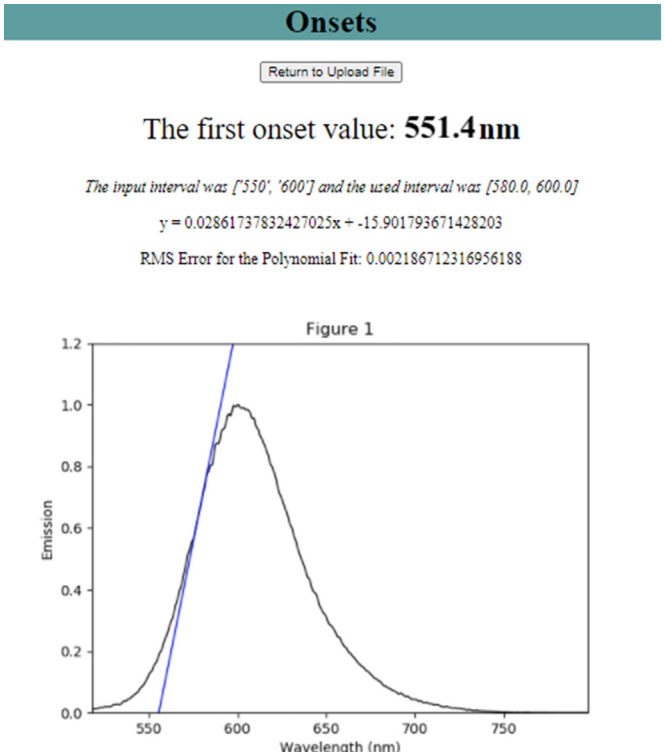

Fig. 6. 0nset determination of λ_{onset} emission for $Ru(bpy)_3Cl_2$.

5. Conclusions

Previous λ_{onset} values are in error from accurately computed x-intercepts of lines tangent to the inflection point of the lowest energy λ_{max} by an average of −2 nm. While, this is not a tremendous error, this present analysis shows that for the sample set, human error tends to lean towards longer wavelength values artificially decreasing the associated E_g^{opt} and optical energy gaps by as much as 5%. The percent errors between the human-derived and computed λ_{onset} are typically within 1%, but future analysis could benefit from a more robust and, most notably, more consistent approach for determining the onset value, especially for applications to shorter wavelengths and higher energies into the UV region like those for $Mn(bpy)(CO)_3Br$, $Ir(ppy)_3$, and $Mn(bpy)_2Br_2$ reported herein.

Finally, this program makes use of standard .csv files, is built on an HTML interface, is available for the both the Windows and Unix-based operating systems, and is freely downloadable via GitHub. This provides easy access and usage to experimental groups who are determining the spectra of novel, synthesized compounds with application to next-generation optical materials. Most importantly, this software has the potential to unify how λ_{onset} values are obtained since very often these are only estimated by simply looking (without even human-drawn tangents), which is often a point of discussion about how the value is obtained since methods can vary widely between research teams.

Declaration of Competing Interest

The authors declare that they have no known competing financial interests or personal relationships that could have appeared to influence the work reported in this paper.

CRediT authorship contribution statement

Austin M. Wallace: Conceptualization, Methodology, Software, Validation, Formal analysis, Investigation, Data curation, Writing - original draft, Writing - review & editing, Visualization. **Christine Curiac:** Methodology, Validation, Formal analysis, Investigation, Data curation, Writing - original draft, Writing - review & editing, Visualization. **Jared H. Delcamp:** Conceptualization, Methodology, Validation, Formal analysis, Resources, Data curation, Writing - original draft, Writing - review & editing, Visualization, Supervision, Project administration, Funding acquisition. **Ryan C. Fortenberry:** Conceptualization, Methodology, Validation, Formal analysis, Resources, Data curation, Writing - original draft, Writing - review & editing, Visualization, Supervision, Project administration, Funding acquisition.

Acknowledgement

This work is supported by NSF Grant OIA-1757220. The 0nset program and all associated documentation is available via https://github.com/Awallace3/0nset/.

Supplementary material

Supplementary material associated with this article can be found, in the online version, at doi:10.1016/j.jqsrt.2021.107544.

References

[1] Choi WS, Seo SSA, Lee HN. Epitaxial growth of complex metal oxides. Amsterdam: Elsevier; 2015. p. 331–63.
[2] Cifuentes MP, Humphrey MG, McGrady JE, Smith PJ, Stranger R, Murray KS, Moubaraki B. High nuclearity ruthenium carbonyl cluster chemistry: 5. Local density functional, electronic spectroscopy, magnetic susceptibility, and electron paramagnetic resonance studies on (carbido)decaruthenium carbonyl clusters. J Am Chem Soc 1997;119:2647–55.
[3] Delcamp JH, Yella A, Nazeeruddina MK, Grätzela M. Modulating dye $E_{(S^+/S^*)}$ with efficient heterocyclic nitrogen containing acceptors for DSCs. Chem Comm 2012;48:2295–7.
[4] García Santander CM, Gómez Rueda SM, de Lima da Silva N, de Camargo CL, Kieckbusch TG, Wolf Maciel MR. Measurements of normal boiling points of fatty acid ethyl esters and triacylglycerols by thermogravimetric analysis. Fuel 2012;92:158–61.
[5] Kolb G, Scheiber S, Antrekowitsch H, Uggowitzer P, Pöschmann D, Pogatscher S. Differential scanning calorimetry and thermodynamic predictions - a comparative study of Al-Zn-Mg-Cu alloys. Metals 2016;6:180.
[6] Fabian DM, Ardo S. Hybrid organic-inorganic solar cells based on bismuth iodide and 1,6-hexanediammonium dication. J Mater Chem A 2016;4:6837–41.
[7] P Makula MP, Macyk W. How to correctly determine the band gap energy of modified semiconductor photocatalysts based on UV-vis spectra. J Phys Chem Lett 2018;9:6814–17.
[8] Carey PH, Ren F, Hays DC, Gila BP, Pearton SJ, Jang S, Kuramata A. Band offsets in ITO/Ga_2O_3 heterostructures. Appl Surface Sci 2017;422:179–83.
[9] Egdell RG, Rebane J, Walker TJ. Competition between initial- and final-state effects in valence- and core-level x-ray photoemission of Sb-doped SnO_2. Phys Rev B 1999;59:1792–9.
[10] Zhang T, Hossain MA, Lee C-Y, Zakaria Y, Abdallah AA, Hoex B. Atomic layer deposited $Zn_xNi_{1-x}O$: a thermally stable hole selective contact for silicon solar cells. Appl Phys Lett 2018;113:262102.
[11] Arantes C, Scholz M, Schmidt R, Dehm V, Rocco MLM, Schöll A, Reinert F, Würthner F. Comparative analysis of the energy levels of planar and core-twisted perylene bisimides in solution and solid state by UV/VIS, CV, and UPS/IPES. Appl Phys A 2012;108:629–37.
[12] Liu SY, Chang JH, Wu IW, Wu CI. Alternating current driven organic light emitting diodes using lithium fluoride insulating layers. Sci Rep 2014;4:7559.
[13] Terashima M, Miyayama T, Shirao T, Mo HW, Hatae Y, Fujimoto H, Watanabe K. The electronic band structure analysis of OLED device by means of in situ LEIPS and UPS combined with GCIB. Surf Interface Anal 2020;52:948–52. doi:10.1002/sia.6777.
[14] Benfield RE. Physics and chemistry of metal cluster compounds. Amsterdam: Kluwer Academic Publishers; 1994. p. 249–70.
[15] Gayton JN, Autry S, Fortenberry RC, Hammer NI, Delcamp JH. Counter anion effect on the photophysical properties of emissive indolizine-cyanine dyes in solution and solid state. Molecules 2018;23:3051.
[16] Ernst RR. Computational aspects of the study of biological macromolecules by nuclear magnetic resonance spectroscopy. Berlin: Springer; 1991. p. 1–25.

[17] Hays PA, Thompson RA. A processing method enabling the use of peak height for accurate and precise proton NMR quantitation. Magn Res Chem 2009;47:819–24.
[18] Naveen Dharmagunawardhane HA, Woerner WR, Wu Q, Huang H, Chen X, Orlov A, Khalifah PG, Parise JB. Photocatalytic hydrogen evolution using nanocrystalline gallium oxynitride spinel. J Mater Chem A 2014;2:19247–52.
[19] Gayton J, Autry SA, Meador W, Parkin SR, H JGA, Hammer NI, Delcamp JH. Indolizine-cyanine dyes: near infrared emissive cyanine dyes with increased stokes shifts. J Org Chem 2019;84:687–97.
[20] Brogdon P, Giordano F, Puneky GA, Dass A, Zakeeruddin SM, Nazeeruddin MK, Grtzel M, Tschumper GS, Delcamp JH. A computational and experimental study of thieno[3,4]thiophene as a proaromatic π bridge in dye-sensitized solar cells. Chem Eur J 2015;22:694–703.
[21] Rodrigues RR, Peddapuram A, Dorris AL, Hammer NI, Delcamp JH. Thienopyrroledione-based photosensitizers as strong photoinduced oxidants: oxidation of $Fe(bpy)_3^{2+}$ in a $>$ 1.3 V dye-sensitized solar cell. ACS Appl Energy Mater 2019;2:5547–56.
[22] McNamara LE, Rill TA, Huckaba AJ, Ganeshraj V, Gayton J, Nelson RA, Sharpe EA, Dass A, Hammer NI, Delcamp JH. Indolizine-squaraines: NIR fluorescent materials with molecularly engineered stokes shifts. Chem Eur J 2017;23:12494.
[23] Rathnamalala CSL, Gayton JN, Dorris AL, Autry SA, Meador W, Hammer NI, Delcamp JH, Scott CN. Donor-acceptor-donor NIR II emissive rhodindolizine dye synthesized by C-H bond functionalization. J Org Chem 2019;84:13186–93.
[24] Shirley H, Parkin S, Delcamp JH. Photoinduced generation of a durable thermal proton reduction catalyst with in situ conversion of $Mn(bpy)(CO)_3Br$ to $Mn(bpy)_2Br_2$. Inorg Chem 2020;59:11266–72.
[25] Meador WE, Autry SA, Bessetti RN, Gayton JN, Flynt AS, Hammer NI, Delcamp JH. Water-soluble NIR absorbing and emitting indolizine cyanine and indolizine squaraine dyes for biological imaging. J Org Chem 2020;85:4089–95.
[26] Huckaba AJ, Shirley H, Lamb RW, Guertin S, Autry S, Cheema H, Talukdar K, Jones T, Jurss JW, Dass A, Hammer NI, Schmehl RH, Webster CE, Delcamp JH. A mononuclear tungsten photocatalyst for H_2 production. ACS Catal 2018;8:4838–47.
[27] Cheema H, Watson J, Peddapuram A, Delcamp JH. A 25 mA cm^{-2} dye-sensitized solar cell based on a near-infrared-absorbing organic dye and application of the device in SSM-DSCs. Chem Commun 2020;56:1741–4.
[28] Rodrigues RR, Boudreaux C, Papish ET, Delcamp JH. Photocatalytic reduction of CO_2 to CO and formate: do reaction conditions or ruthenium catalysts control product selectivity? ACS Appl Energy Mater 2019;2:37–46.